Journal of Offshore Mechanics and Arctic Engineering. Received April 04, 2022;
Accepted manuscript posted September 01, 2022. doi:10.1115/1.4055552

LQR optimal control of two-rotor wind turbine mounted on spar-type floating platform

Omar El Beshbichi[a,*], Yihan Xing[a], Muk Chen Ong[a]

[a]*Department of Mechanical and Structural Engineering and Materials Science, University of Stavanger, Stavanger, Norway.*

Abstract

Interest is steadily growing for multi-rotor wind turbine concepts. This type of wind turbine offers a practical solution for scaling issues of large wind turbine components and for the reduction of costs associated with manufacturing, logistics, and maintenance. However, the literature lacks thorough knowledge of the dynamic performance of multi-rotor wind turbine concepts installed on floating platforms. Previous research studied the dynamic response of a two-rotor wind turbine concept mounted on a spar-type floating platform (2WT). Platform yaw motion is a significant dynamic factor directly caused by differential turbulence intensity experienced by the two hubs coupled with the distribution of thrust loads on the tower structure. Blade-pitch control analysis also showed how the 2WT yaw response is extremely sensitive to the control strategy employed. In this work, a linear quadratic regulator (LQR) is used to design an optimal controller for the 2WT prototype. Three LQR gain schedules corresponding to three operation regions are considered. An in-house tool for the dynamic analysis of multi-rotor floating wind turbines is used for linear state-space extraction and dynamic analysis. The control performance in different load conditions is assessed against the baseline OC3 PI control strategy and a PI-P control strategy in a previous paper presented by the authors.

Keywords: Linear quadratic regulator (LQR), Offshore Wind, Spar, Floating wind turbines, Multi-rotor, Optimal control.

1. Introduction

The installed capacity of offshore wind energy has steadily increased in the last decade. Estimates from the global wind energy council (GWEC) account for a total installed capacity offshore of about 35 GW in 2021 out of a total wind energy capacity of about 600 GW [1]. Space availability, stronger and steadier winds, and less interference with populated areas, to name but a few reasons for the appeal of offshore wind installations [2]. Almost all of the offshore wind turbines currently installed are bottom-fixed. However, most wind potential is beyond the limit imposed by the maximum water depth at which bottom-fixed structures are economically feasible (around 50 m). Floating offshore wind turbines (FOWT) have been proposed as a technical solution, and several examples of FOWTs

*Corresponding author
Email address: omar.elbeshbichi@uis.no (Omar El Beshbichi)

Journal of Offshore Mechanics and Arctic Engineering. Received April 04, 2022;
Accepted manuscript posted September 01, 2022. doi:10.1115/1.4055552

deployment are present [3, 4]. Multi-rotor FOWTs have also been proposed, where the advantages are associated with more economical offshore operations and floating platform sharing. Two commercial examples of multi-rotor FOWTs currently under development are TwinWind™ by Hexicon [5] and Flex2power by Rosenberg Worley AS [6]. The former is a two-rotor wind turbine mounted on a semisubmersible platform. Hexicon has recently signed an agreement for conditional site exclusivity with a reservation of 6 MW for deploying a demonstrator prototype at the Metcentre's deepwater site off Norway's coast [7]. Flex2power, on the other hand, is a modularized concept for combined wind, wave, and sun energy production. Another innovative twin-rotor floating wind technology is Nezzy^2, currently under development by EnBW and the North German engineering company Aerodyn Engineering [8, 9] and composed of two wind turbines supported by a Y-shaped semi-submersible platform anchored by six mooring lines [10]. A 1:10 scale prototype has been recently tested in two-blades and three-blades variants. To date, the literature lacks knowledge on the dynamic performance of multi-rotor FOWTs systems. Recent research evaluated the dynamic response of a two-rotor wind turbine prototype mounted on a spar-type floating platform (2WT) [11]. The concept was first defined as a first-attempt prototype by seeking simplicity of platform design, great availability of data concerning similar platform performance in the literature, and easy result assessment. It was found that the 2WT design is subject to significant platform yaw motion associated with differential turbulence intensity at the hubs coupled with the distribution of thrust loads on the tower structure. A simple proportional control (PI-P) mitigating yaw motion was introduced in parallel with the baseline OC3 proportional-integral (OC3 PI) controller, significantly reducing platform yaw response. Figure 1 presents the 2WT system. The design considers two baseline NREL 5 MW wind turbines [12]. Major system parameters are listed in Table 1. Three catenary mooring lines are considered for station-keeping, placed at 120 deg from one another starting from the downwind position. The mooring lines mass density is 200 kg/m, the static vertical length is about 250 m, and the unstretched static length is about 900 m. Additional concentrated stiffness in the platform yaw direction of about 9.8e7 Nm/rad is considered to account for yaw stiffness given by the delta line configuration [12]. Hydrostatic quantities are relative to the static position of the system affected by the loading of the mooring lines. Table 2 lists the natural frequencies and damping ratios from logarithmic decrement of the 2WT system computed through free-decay tests. Control of variable-speed wind turbines is achieved by regulating blade-pitch angles and generator torque [13]. Control is generally divided into four regions as a function of control objective:

- Region 1. Below cut-in wind speed. In this region, no generator torque allows drivetrain acceleration for start-up.
- Region 2. Between cut-in wind speed and rated wind speed. In this region, aerodynamic power is optimized by regulating generator torque.
- Region 3. Between rated and cut-out wind speed. In this region, generator speed is maintained equal to the rated value by actuating blade-pitch angles. Generator torque control allows for either constant electric power output or constant generator torque.

- Cut-off region. Above cut-out wind speed. In this region, blades are fully pitched for parking the wind turbine by disrupting the aerodynamic loads.

The most common blade-pitch control implementation is employing a PI logic, for instance, in the case of the baseline OC3 PI controller [12]. A linear quadratic regulator (LQR) may also be employed to design the control of FOWTs [14, 15]. Pham et al. [16] designed an LQR control for a multi-MW wind turbine. Christiansen et al. [17, 18] designed and analyzed an LQR controller applied to a spar-type FOWT.

This work presents the design of an LQR control for the 2WT system. Control objectives are the reduction of platform yaw motion while regulating the generators' speed. To date, no other examples of the employment of LQR as optimal control algorithm for mitigating platform yaw response in multi-rotor FOWTs is present in the literature. Results are compared against 2WT performance controlled with the baseline OC3 PI controller and the coupled PI-P controlled as defined in [11].

2. 2WT dynamic model

Dynamic assessment and linear state-space extraction for the 2WT prototype are performed through an in-house tool developed in Modelica (v3.2.3) [19]. Modelica is a non-proprietary, declarative, object-oriented language developed by the non-profit Modelica Association and used to conveniently model multi-domain systems [20]. The open-source Modelica-based platform OpenModelica is also used for development (v1.16.2) [21].

2.1. Nonlinear model

Nonlinear dynamic analysis of the floating system assumes linear (Airy) hydrodynamics [22]. This assumption is valid in most practical cases, i.e., when the wave height is much smaller than the water depth. The frequency-domain hydrodynamic problem associated with the platform design is solved through the commercial code WADAM within DNV SESAM [23]. The 2WT system is assumed to be a single rigid body with six degrees of freedom (DoF). The motions are then computed using rigid equations of motion [12]:

$$[M]\underline{\ddot{q}} + [C]\underline{q} + C_{0,3} = -[A]_{inf}\underline{\ddot{q}} - \int_0^t [K(t-\tau)]\underline{\dot{q}}d\tau + \underline{F}_w + \underline{F} + \underline{F}_m + \underline{F}_g \tag{1}$$

where $\underline{q}$ are the platform DoFs, $[M]$ is the total inertia tensor of the 2WT system, $[C]$ is the hydrostatic matrix, $C_{0,3}$ is the Archimede restoring load, $[A]_{inf}$ is the added mass term from hydrodynamic radiation computed at infinite wave frequency, $[K(t)]$ is the retardation-kernel matrix from hydrodynamic radiation, $\underline{F}_w$ are the loads from incident waves, $\underline{F}$ are the aerodynamic loads, $\underline{F}_m$ are the mooring loads, and $\underline{F}_g$ are the gravitational loads. Station-keeping loads from mooring lines are included by means of a non-linear quasi-static formulation, i.e., the effect of the acceleration and velocity of the mooring lines on station-keeping loads is disregarded. Aerodynamic loads are assumed composed of concentrated thrusts acting at the hubs and torques acting on the dynamics of the drivetrain. Additional DoFs are

added to account for drivetrains dynamics and used to define the aerodynamic state of the system. Drivetrain dynamics is described as:

$$(I_r + \gamma^2 I_g)\dot{\omega}_r = T - \gamma T_g \tag{2}$$

where I_r is the rotor moment of inertia, I_g is the generator moment of inertia, γ is the gearbox ratio, ω_r is the low-speed shaft speed, T is the aerodynamic torque, and T_g is the generator torque. Aerodynamic loads are computed utilizing steady-state aerodynamic coefficients associated with the onshore NREL 5 MW wind turbine design. Aerodynamic coefficients of thrust, torque, and aerodynamic power are collected in FAST and Figures 2, 3, and 4 show the resulting mapping [where $\lambda = \omega_r R/U_{rel}$ is the tip speed ratio (TSR), U_{rel} is the relative wind velocity at the hub, and β is the rotor-collective blade-pitch angle]. Aerodynamic loads are computed as:

$$F = \frac{1}{2}\rho_{air} C_T(\lambda,\beta) A {U_{rel}}^2 \tag{3}$$

and:

$$T = \frac{1}{2}\rho_{air} R C_Q(\lambda,\beta) A {U_{rel}}^2 \tag{4}$$

where ρ_{air} is the air density, C_T is the thrust coefficient, C_Q is the torque coefficient, A is the rotor-swept area, and R is the rotor radius. The effect of platform motion on the relative wind speed at the hub affects the computation of the TSR and the aerodynamic thrust and torque loads. Turbulent wind profiles are computed in TurbSim [24]. The dynamic response of the blade-pitch actuation system is described through a second-order transfer function (f_n = 5 Hz, ξ = 0.02).

Even though previous work demonstrated that the method is sufficiently accurate to determine the general dynamic response of FOWTs [19, 25], more complex aerodynamic effects cannot be assessed. For instance, the aerodynamic interaction between rotors is not available. Concentrated loads effectively neglect wind shear. The effect of platform yaw motion on the aerodynamic performance of the wind turbine is also not directly assessed, as well as aerodynamic drag loads on the tower and the aerodynamic effects of the tower's proximity on the turbine blades. These effects may be significant and should later be investigated to determine optimal control weights.

2.2. Linear model

The nonlinear model can be described as:

$$\begin{aligned} \dot{\underline{x}} &= f(\underline{x}, \underline{u}) \\ \underline{y} &= g(\underline{x}, \underline{u}) \end{aligned} \tag{5}$$

where $\underline{x}$ is the state vector, $\underline{u}$ is the input vector, $\underline{y}$ is the output vector, f is the nonlinear relationship describing the dynamic behavior of the system, and g is the nonlinear output function [26]. Control design exploits the linearization of the system by using first order Taylor expansion about the neighborhood of a steady-state operation point. If $\underline{x}^*$ is the state vector at the operation point and $\tilde{\underline{x}}$ the infinitesimal variation about the operation point (such that $\underline{x} = \underline{x}^* + \tilde{\underline{x}}$)

the linear system can be expressed as:

$$\begin{aligned} \dot{\underline{\tilde{x}}} &= [A]\underline{\tilde{x}} + [B]\underline{\tilde{u}} \\ \underline{\tilde{y}} &= [C]\underline{\tilde{x}} + [D]\underline{\tilde{u}} \end{aligned} \tag{6}$$

where $[A] = \left.\frac{\partial f(\underline{x},\underline{u})}{\partial \underline{x}}\right|_{\underline{x}=\underline{x}^*}$, $[B] = \left.\frac{\partial f(\underline{x},\underline{u})}{\partial \underline{u}}\right|_{\underline{u}=\underline{u}^*}$, $[C] = \left.\frac{\partial g(\underline{x},\underline{u})}{\partial \underline{x}}\right|_{\underline{x}=\underline{x}^*}$ and $[D] = \left.\frac{\partial g(\underline{x},\underline{u})}{\partial \underline{u}}\right|_{\underline{u}=\underline{u}^*}$ are the Jacobian matrices of the system evaluated at the operation point. Jacobian components describe sensitivity relationships among states, inputs, and outputs. Modelica models can be linearized in OpenModelica by calling the function *linearize()* in the OMShell and specifying the simulation time at which linearization occurs. Only significant platform states have been enabled in the linearization process. Moreover, no wave loads are considered and radiation damping states are disabled. The state vector considered is:

$$\underline{\tilde{x}} = [\beta_L, \beta_R, \dot{\beta_L}, \dot{\beta_R}, \Omega_L, \Omega_R, q_5, \dot{q_5}, q_6, \dot{q_6}] \tag{7}$$

where Ω is the rotor speed, q_5 is the platform pitch angle, and q_6 is the platform yaw angle. Subscripts L and R stand for the left and right rotor, respectively. The input vector considered is:

$$\underline{\tilde{u}} = [\beta_L, \beta_R] \tag{8}$$

Moreover, external wind speed is considered as additional system input [27]:

$$\underline{\tilde{u}}_d = [U_{rel}] \tag{9}$$

Above-rated steady-state error of the rotor speed can be avoided by including states expressing the integral error between the reference and actual speed, as in linear-quadratic regulators with integral terms (LQI) [28]. Keeping LQI notation, the output variables are simply defined as the generators' speed:

$$\underline{\tilde{y}} = [\Omega_L, \Omega_R] \tag{10}$$

The integral error can be defined as:

$$\underline{\Omega}_{err} = \int_0^t (\Omega_{ref} - \underline{\tilde{y}})\, dt \tag{11}$$

where Ω_{ref} is the reference (rated) rotor speed. From equations 6 and 11 (and assuming $[D] = [0]$) it follows:

$$\dot{\underline{\Omega}}_{err} = \Omega_{ref} - [C]\underline{\tilde{x}} \tag{12}$$

The augmented system can finally be obtained as:

$$\begin{Bmatrix} \dot{\underline{\tilde{x}}} \\ \dot{\underline{\Omega}}_{err} \end{Bmatrix} = \begin{bmatrix} A & 0 \\ -C & 0 \end{bmatrix} \begin{Bmatrix} \underline{\tilde{x}} \\ \underline{\Omega}_{err} \end{Bmatrix} + \begin{bmatrix} B \\ 0 \end{bmatrix} \underline{\tilde{u}} + \begin{bmatrix} B_d \\ 0 \end{bmatrix} \underline{\tilde{u}}_d + \begin{bmatrix} 0 \\ \Omega_{ref} \end{bmatrix} \tag{13}$$

which in compact form becomes:

$$\dot{\underline{\tilde{x}}}_T = [A_T]\underline{\tilde{x}}_T + [B_T]\underline{\tilde{u}} + [B_{d,T}]\underline{\tilde{u}}_d + [E] \tag{14}$$

Journal of Offshore Mechanics and Arctic Engineering. Received April 04, 2022;
Accepted manuscript posted September 01, 2022. doi:10.1115/1.4055552

where $\underline{\tilde{x}}_T$ is the global state vector:

$$\underline{\tilde{x}}_T = [\beta_L, \beta_R, \dot{\beta_L}, \dot{\beta_R}, \Omega_L, \Omega_R, q_5, \dot{q_5}, q_6, \dot{q_6}, \Omega_{L,err}, \Omega_{R,err}] \tag{15}$$

The final state-space system is hence composed of 12 states.

3. Control design

3.1. LQR blade pitch control design

LQR control is based on the minimization of a quadratic cost function accounting for state control and control input usage [26]:

$$J = \int_{t_0}^{t_1} (\underline{\tilde{x}}_T^T [Q] \underline{\tilde{x}}_T + \underline{\tilde{u}}^T [R] \underline{\tilde{u}})\, dt \tag{16}$$

where $[Q]$ and $[R]$ are symmetric positive semi-definite and positive definite weight matrices, respectively. The selection of weight parameters is typically left to the control system designer and is often resolved by rule of thumb or exhaustive search approaches. Sensitivity analysis and optimization methods may be employed to determine optimal weight parameters which maximize the control system performance according to the selected objectives [29]. In this work, weight matrices are determined heuristically by considering the associated control objectives and evaluating the ensuing system's performance. The full-state feedback minimizing J is given by:

$$\underline{\tilde{u}} = -[K] \underline{\tilde{x}}_T \tag{17}$$

where $[K]$ is the control gain matrix given by:

$$[K] = [R]^{-1} [B_T]^T [P] \tag{18}$$

where $[P]$ is a positive definite symmetric matrix obtained by solving the algebraic Riccati equation (ARE):

$$[A_T]^T [P] + [P][A_T] - [P][B_T][R]^{-1} [B_T]^T [P] + [Q] = 0 \tag{19}$$

LQR design is carried out in MATLAB by using the featured LQR function *lqr*.

3.2. Generator torque control

The generator torque control is excluded from linear control design, and a standard control schedule is employed in parallel as shown in Figure 5. Each wind turbine is controlled independently. Figure 6 shows the controlled generator torque as a function of generator speed. The regions depicted are the standard control regions as described in Introduction. Torque control scheme in Region 2 maximizes the wind turbine aerodynamic power (see Figure 2) for each aerodynamic state [30, 31]:

$$\begin{aligned} T_g &= C\Omega_g^2 \\ C &= \frac{1}{2}\rho_{air} \frac{C_{P,max}(\beta)}{\lambda^*(\beta)^3} \pi R^5 \end{aligned} \tag{20}$$

Journal of Offshore Mechanics and Arctic Engineering. Received April 04, 2022;
Accepted manuscript posted September 01, 2022. doi:10.1115/1.4055552

where Ω_g is the generator speed, λ^* is the optimal TSR at a given blade pitch angle, and $C_{P,max} = C_P(\lambda^*(\beta), \beta)$ is the optimal power coefficient. The blade pitch angle used to determine λ^* and $C_{P,max}$ is at present assumed constant and equal to the global optimal value (0 deg). The assumption is in consequence of small mean and standard deviation values of blade-pitch angles in Region 2 given by the present control design ($\mu \simeq 1$ deg, $\sigma \simeq 2$ deg). Torque control scheme in Region 3 keeps constant generator power output:

$$P_e = T_g \Omega_g \tag{21}$$

where P_e is the rated generator power.

3.3. LQR blade pitch control schedules

The 2WT system is considerably non-linear and exhibits different behavior in Region 2, Region 3, and around the rated wind speed. Moreover, control objectives change in relation to the operation regime considered. Three different LQR control schedules have thus been defined for the rotor-collective blade-pitch control. The operational wind speeds at which each controller operates are listed in Table 3. Control LQR-A operates at below-rated wind regimes (between 3 and 10 m/s). Control LQR-B operates close to the rated wind speed (between 11 and 12 m/s). Finally, control LQR-C operates at above-rated wind speeds (between 13 and 25 m/s). The wind speed gaps between control schedules are associated with transitional conditions not considered in this work. Smooth transitioning between controllers may be employed to effectively automate the controller selection process [32]. This may be achieved by estimating the effective wind speed using a Kalman filter (KF) [33]. As wind speed stationarity is commonly assumed (as in TurbSim [24]), the controller employed is at present simply determined using the mean wind speed used to generate the wind profile realization.

Three different operation points (one for each controller) are used to linearize the system, as listed in Table 4. The control objectives used in this study are 1) the mitigation of platform yaw motion, and 2) the regulation of generators' speed at the rated value for rated and above-rated wind speeds. The employment of as few control objectives as possible has been adopted for two reasons. First, platform yaw motion is an important dynamic mode strictly associated with the 2WT system. Consequently, more emphasis has been given to its mitigation by means of an optimal control strategy. Secondly, fewer control objectives make the evaluation of the control system performance easier since fewer state couplings are taken into account. A much larger number of control objectives can be considered in later control design stages. LQR control objectives are summarized as follows. Control LQR-A minimizes platform yaw motion. Control LQR-B minimizes platform yaw motion while controlling the generators' speed at rated values. Control LQR-C is similar in scope to control LQR-B, but more weight is given to the generator speed control to optimize power output quality.

LQR control weights and associated gains scheduling for each controller are selected heuristically by considering the associated control objectives and evaluating the resulting performance of the system. Values used in this work are listed in Tables 5 and 6.

Journal of Offshore Mechanics and Arctic Engineering. Received April 04, 2022;
Accepted manuscript posted September 01, 2022. doi:10.1115/1.4055552

4. Reference blade pitch controls

4.1. OC3 PI control

The baseline OC3 PI control computes the rotor-collective blade-pitch angle using a gain-scheduled proportional-integral control on the error between generator speed and the rated generator speed value [12]. The control law can be expressed as:

$$\beta = K_P(\beta)(\omega_g - \omega_{g,ref}) + K_I(\beta)\int_0^t (\omega_g - \omega_{g,ref})dt \tag{22}$$

where K_P and K_I are the proportional and integral gains scheduled as a function of the blade pitch angle. Gain scheduling takes into account the nonlinear relationship between blade-pitch and variation of aerodynamic power.

It is known that platform pitch instability may occur if the control system is too stiff. The gains proposed for control of the OC3-Phase IV floating system are designed to reduce the controller natural frequency from 0.6 rad/s (associated with baseline onshore gains) to about 0.2 rad/s – thus lower than the platform pitch natural frequency of about 0.21 rad/s [34]. Reduction of controller frequency below the platform pitch natural period has been proved beneficial for the avoidance of negative damping in the platform pitch direction [35]. Since the 2WT and OC3-Phase IV platform pitch motion natural frequencies are very similar (see Table 2) and the same drivetrain system is used, the same reduced gains can be employed without further modification, as listed in Table 7. No instability occurrence has been detected with this control setup. Moreover, the OC3 PI control configuration applied to the 2WT system may also determine negative damping in the platform yaw direction at above-rated wind speeds. This can be associated with the reduction of thrust at the hub moving upwind induced by higher relative wind speed. This effect may exacerbate the platform yaw motion, which is predominantly induced by wind turbulence intensity [11].

4.2. PI-P control

Previous work focusing on the dynamic response of the 2WT system proposed a simple coupled control strategy aiming at the mitigation of platform yaw motion [11]. This control strategy, called PI-P for brevity, is composed of a proportional control mitigating platform yaw motion superimposed to the baseline OC3 PI control. The control law associated with the proportional control component can be expressed as:

$$\begin{cases} \text{if } L \quad \beta_{q_6} = max(0, -K_{q6}q_6) \\ \\ \text{if } R \quad \beta_{q_6} = max(0, K_{q6}q_6) \end{cases} \tag{23}$$

where β_{q_6} is the blade-pitch angle associated with platform yaw motion control, and K_{q_6} is the associated proportional control gain. This control reduces thrust at the hub experiencing relative motion in the downwind direction. Heuristic control tuning showed best performance at around $K_{q_6} \simeq 1.5$. Table 7 summarizes the controller parameters.

Journal of Offshore Mechanics and Arctic Engineering. Received April 04, 2022;
Accepted manuscript posted September 01, 2022. doi:10.1115/1.4055552

5. Environment

The performance of the LQR control design is assessed by evaluating the fully-coupled nonlinear response of the 2WT system over a wide range of wind speeds at below-rated, rated, and above rated environmental conditions. Results are compared to the performance relative to the OC3 PI control and the coupled PI-P control. Environmental parameters are listed in Table 8. Wind speeds range from a minimum of 5 m/s to the cut-off value of 25 m/s. The turbulence model considered is Kaimal, and a normal turbulence type with characteristic B (NTM - type B) is considered [24]. All hydrodynamic loads are considered, where incident wave loads are relative to irregular waves from the JONSWAP spectrum. The effect of current is neglected. A water depth of about 320 m is considered. Waves are aligned with the wind direction. Only one sea state is applied to the system, corresponding to a characteristic wave height H_s of 6 m and characteristic wave period T_p of 10 s.

6. Results

The integration method *ida* is used to solve the equations of motion of the system. Integration tolerance equal to $1x10^{-4}$ is used. A time interval equal to 0.3 s is used, sufficient to cover rigid motion response. The linear solver *totalpivot* and non-linear solver *kinsol* are also employed. Time realizations of about 4000 s are computed. The first 400 s are removed to avoid numerical transients, leaving a net 1 h simulation time to compute short-term results. A total of five response parameters are used to evaluate the LQR controller response and compare it with reference control strategies [36]. The first parameter is the platform yaw motion. Standard deviation (STD) should be kept as low as possible. The second parameter is generator speed. More stable generator speed leads to higher power quality. The third parameter is the electric power output, which is directly related to the variation of generator speed. The fourth parameter is the platform pitch motion, which can induce significant tower fore-aft (FA) bending loads if too high. Finally, the fifth parameter is the blade pitch rate. This parameter is used as an indication of actuation usage. The assumptions employed in this work may have a significant impact on the performance parameters here considered. For instance, rigid structural dynamics may significantly reduce STD values - especially of generator speed and electric power output. The neglect of the effect of blades' spatial orientation on the aerodynamic loads may also significantly influence platform yaw motion STD. Nonetheless, the results obtained are sufficiently accurate for global dynamic performance evaluation and control system design purposes. A detailed exposition of the dynamic response of the 2WT system will be the subject of future work.

Figure 7 shows the performance of LQR and coupled PI-P controllers as a function of wind speed. Platform yaw motion STD with OC3 PI controller is also included. It is clear that platform yaw motion is significant without a proper control strategy throughout the full wind speed range (OC3 PI). PI-P controller reduces the platform yaw motion significantly. LQR control is found to perform significantly better than the PI-P control, especially at rated and above-rated wind speeds. At below-rated wind speeds the advantage is present but small (about -8% LQR yaw motion STD and -11% LQR pitch motion STD if compared to PI-P response at 8 m/s). This is expected, since the only control

Journal of Offshore Mechanics and Arctic Engineering. Received April 04, 2022;
Accepted manuscript posted September 01, 2022. doi:10.1115/1.4055552

objective of control LQR-A is platform yaw motion reduction, while the major advantage of LQR against PI strategies is the ability to control multiple objectives [27]. At near-rated and above-rated wind speeds the LQR controller performs significantly better than the PI-P controller. The advantage is significant also for operating conditions far from the one used for linearization. At 12 m/s the platform yaw motion STD is about -58% and the platform pitch motion STD is about -40% if compared to the PI-P controller. Marginally higher mean platform pitch motion is obtained around the rated wind speed (about +5% if compared to PI-P controller). LQR performance is stable also at very high wind speeds. Electric power quality is also increased with the LQR control. At 17 m/s, the electric power output mean and STD difference if compared to the PI-P control is about +100 kW and -17%, respectively. Excellent generator speed control at above-rated wind speeds is obtained, with a significant STD reduction obtained with the LQR controller (about -25% if compared to the PI-P controller). It can also be noted how the average generator speed reaches close-to-rated values at about 11 m/s, while the average electric power output stabilizes at close-to-rated values at about 13 m/s. This discrepancy is mainly associated with the relatively higher electric power STD close to the rated wind speed (17% of the mean value against the 5% associated with the generator speed). This can further be related to the fluctuating aerodynamic torque at the low-speed shaft given by wind turbulence.

Figure 8 and Figure 9 show time realizations of about 300 s of the 2WT response for LQR, the baseline OC3 PI, and the coupled PI-P controllers for above-rated (13 m/s) and below-rated (9 m/s) wind speed conditions, respectively. LQR control yields more stable results in terms of platform yaw and pitch motions. LQR controller is able to reduce peak variations of generator speed from the rated value. It can be also noted that the blade pitch angle experiences a higher rate of change, associated with a more onerous actuator usage. The increase in blade pitch rate is not problematic, as long as subsequent detailed investigation of the loads and fatigue assessment associated with the blade pitch actuation system are carried out.

It is clear how the LQR controller gives most of its advantages around and above the rated wind speed. Four response parameters are used to further evaluate the LQR controller response and compare it with reference controllers. Response evaluation is given in terms of the root mean square (RMS) of platform yaw motion, generator speed error, electric power error, and blade-pitch rate. Figure 10 shows the performance comparison for LQR, the baseline OC3 PI, and the coupled PI-P controllers at above-rated wind speeds. Moreover, Figure 11 shows the performance comparison for LQR, the baseline OC3 PI, and the coupled PI-P controllers at below-rated wind speeds. At above-rated wind speeds, LQR is the best performing controller. The PI-P controller leads to higher speed and power errors than the OC3 PI controller at higher wind speeds (about +10% RMS power error difference at 17 m/s). Performance must, however, be paid in terms of a higher actuation usage. The RMS of blade-pitch rate is significantly higher for the LQR controller (about +27% and +35% if compared to PI-P and OC3 PI controllers at 13 m/s, respectively). However, the increase in blade-pitch rate is well within the limits imposed by actuation rate saturation (max 8 deg/s [12]). At below-rated wind speeds, the LQR and PI-P performance is similar.

7. Conclusion

This work presented the design of an optimal LQR controller for a two-rotor floating wind turbine prototype. Three different LQR control schedules were defined, associated to below-rated, near-rated, and above-rated wind speeds. For each controller, a related operational point was used for linearization. Numerical evaluations were used to assess the performance of the LQR controller against the performance of baseline OC3 PI and coupled PI-P controllers. Suited control objectives were considered. It was shown how the LQR controller performs significantly better than both reference controllers. The advantage was found to be most significant at above-rated wind speeds. Platform yaw and pitch motion STD is reduced considerably. Mean platform pitch motion close to the rated wind speed is marginally higher for the LQR controller than the PI-P performance. Electric power output STD is also reduced, indicating higher power quality. Greater performance must be paid for higher actuator usage (estimated in terms of blade-pitch rate RMS). Nevertheless, peak values are well within saturation limits.

Acknowledgment

This PhD project is financed by the Equinor Akademia Program at the University of Stavanger.

References

[1] GWEC, *Global Wind Report 2021*, 2021. [Online]. Available: https://gwec.net/market-intelligence/resources/

[2] J. Cruz and M. Atcheson, *Floating Offshore Wind Energy - The Next Generation of Wind Energy*. Springer, 2016.

[3] Equinor, *Hywind Scotland Pilot Park - Environmental Statement, Non Technical Summary*, 2015.

[4] Principle Power, *The WindFloat: Enabling a Paradigm Shift in Offshore Wind*, 2016.

[5] Hexicon, *Operations Update Q2 2021*, 2021.

[6] Flex2Power, *Official Website (Accessed: July 2022)*, 2022. [Online]. Available: https://flex2power.com/

[7] Hexicon, *Press release - Hexicon to develop TwinWay project for floating wind in Norway*, 2021.

[8] EnBW, *Official Website (Accessed: July 2022)*, 2021. [Online]. Available: https://www.enbw.com/company/

[9] Aerodyn Engineering, *Official Website (Accessed: July 2022)*, 2021. [Online]. Available: https://aerodyn-engineering.com/products/nezzy-technology/

[10] EnBW, *Floating wind turbine: Nezzy2 - Website (Accessed: July 2022)*, 2021. [Online]. Available: https://www.enbw.com/renewable-energy/wind-energy/our-offshore-wind-farms/nezzy2-floating-wind-turbine/

[11] El Beshbichi O., Xing Y., and Ong M. C., "Dynamic analysis of two-rotor wind turbine on spar-type floating platform," *Ocean Engineering*, vol. 236, p. 109441, 2021, doi: https://doi.org/10.1016/j.oceaneng.2021.109441.

[12] Jonkman J., *Dynamics Modeling and Loads Analysis of an Offshore Floating Wind Turbine*, 2007, doi: https://doi.org/10.2172/921803.

[13] Bossanyi E. A., "The design of closed loop controllers for wind turbines," *Wind Energy*, vol. 3, no. 3, pp. 149–163, 2000, doi: https://doi.org/10.1002/we.34.

[14] Wright A. D. and Fingersh L. J., "Advanced control design for wind turbines; part i: Control design, implementation, and initial tests," 2008, doi: https://doi.org/10.2172/927269.

[15] Stol K. A. and Fingersh L. J., "Wind turbine field testing of state-space control designs: August 25, 2003–november 30, 2003," 2004, doi: https://doi.org/10.2172/15009600.

[16] Pham T. K., Nam Y., Kim H., and Son J., "Lqr control for a multi-mw wind turbine," *International Journal of Mechanical and Mechatronics Engineering*, vol. 6, no. 2, pp. 507 – 512, 2012, doi: https://doi.org/10.5281/zenodo.1062490.

[17] Christiansen S., Knudsen T., and Bak T., "Optimal control of a ballast-stabilized floating wind turbine," in *2011 IEEE International Symposium on Computer-Aided Control System Design (CACSD)*, 2011, pp. 1214–1219, doi: https://doi.org/10.1109/CACSD.2011.6044574.

[18] Christiansen S., Knudsen T., and Bak T., "Extended onshore control of a floating wind turbine with wave disturbance reduction," *Journal of Physics: Conference Series (Online)*, vol. 555, no. 1, pp. 1–10, 2014, doi: https://doi.org/10.1088/1742-6596/555/1/012018.

[19] El Beshbichi O., Xing Y., and Ong M. C., "An object-oriented method for fully coupled analysis of floating offshore wind turbines through mapping of aerodynamic coefficients," *Marine Structures*, vol. 78, p. 102979, 2021, doi: https://doi.org/10.1016/j.marstruc.2021.102979.

[20] The Modelica Association, *Modelica® - A Unified Object-Oriented Language for Systems Modeling. Language Specification, Version 3.4*, 2017.

[21] OSMC, *OpenModelica User's Guide. Release v1.19.0*, 2021.

[22] Faltinsen O., *Sea loads on ships and offshore structures*, 1990. [Online]. Available: https://www.osti.gov/biblio/5464335

[23] DNV, *WADAM - Wave Analysis by Diffraction and Morison theory. SESAM User Manual*, 2017.

[24] Jonkman B. J., *TurbSim user's guide: version 1.50*, 2009, doi: https://doi.org/10.2172/965520.

[25] Karimirad M. and Moan T., "A simplified method for coupled analysis of floating offshore wind turbines," *Marine Structures*, vol. 27, no. 1, pp. 45–63, 2012, doi: https://doi.org/10.1016/j.marstruc.2012.03.003.

[26] Prasad L. B., Tyagi B., and Gupta H. O., "Optimal control of nonlinear inverted pendulum system using pid controller and lqr: Performance analysis without and with disturbance input," *International Journal of Automation and Computing*, vol. 11, pp. 661–670, 2014.

[27] Kumar A. and Stol K. A., "Simulating feedback linearization control of wind turbines using high-order models," *Wind Energy*, vol. 13, pp. 419–432, 2009.

[28] Feng Z., Zhu J., and Allen R., "Design of continuous and discrete lqi control systems with stable inner loops," *Journal of Shanghai Jiaotong University (Science)*, vol. 12, no. 6, pp. 787–792, 2007.

[29] K. Miyamoto, J. She, D. Sato, and N. Yasuo, "Automatic determination of lqr weighting matrices for active structural control," *Engineering Structures*, vol. 174, pp. 308–321, 2018, doi: https://doi.org/10.1016/j.engstruct.2018.07.009.

[30] Johnson K. E., "Adaptive torque control of variable speed wind turbines," 2004, doi: https://doi.org/10.2172/15008864.

[31] Johnson K. E., Fingersh L. J., Balas M. J., and Pao L. Y., "Methods for Increasing Region 2 Power Capture on a Variable-Speed Wind Turbine," *Journal of Solar Energy Engineering*, vol. 126, no. 4, pp. 1092–1100, 2004, doi: https://doi.org/10.1115/1.1792653.

[32] Lindeberg E., Svendsen H. G., and Uhlen K., "Smooth transition between controllers for floating wind turbines," *Energy Procedia*, vol. 24, pp. 83–98, 2012, doi: https://doi.org/10.1016/j.egypro.2012.06.090.

[33] Jena D. and Rajendran S., "A review of estimation of effective wind speed based control of wind turbines," *Renewable and Sustainable Energy Reviews*, vol. 43, pp. 1046–1062, 2015, doi: https://doi.org/10.1016/j.rser.2014.11.088.

[34] Jonkman J., *Definition of the Floating System for Phase IV of OC3*, 2010, doi: https://doi.org/10.2172/979456.

[35] Larsen T. J. and Hanson T. D., "A method to avoid negative damped low frequent tower vibrations for a floating, pitch controlled wind turbine," *Journal of Physics: Conference Series*, vol. 75, p. 012073, 2007, doi: https://doi.org/10.1088/1742-6596/75/1/012073.

[36] Sarkar S., Fitzgerald B., and Basu B., "Individual blade pitch control of floating offshore wind turbines for load mitigation and power regulation," *IEEE Transactions on Control Systems Technology*, vol. 29, no. 1, pp. 305–315, 2021, doi: https://doi.org/10.1109/TCST.2020.2975148.

Journal of Offshore Mechanics and Arctic Engineering. Received April 04, 2022;
Accepted manuscript posted September 01, 2022. doi:10.1115/1.4055552

List of Tables

Table 1: System parameters [11, 12].

Diameter at SWL	m	7.6
Diameter	m	10.5
Draft	m	140
Depth to COG	m	100.9
Water Displacement	m^3	$11.7x10^3$
Platform Mass (including ballast)	kg	$10.6x10^6$
Platform Roll Moment of Inertia	kgm^2	$1.13x10^{10}$
Platform Pitch Moment of Inertia	kgm^2	$1.13x10^{10}$
Platform Yaw Moment of Inertia	kgm^2	$1.7x10^8$
Heave Hydrostatic stiffness	N/m	$4.56x10^5$
Roll Hydrostatic stiffness	Nm/rad	$3.42x10^9$
Pitch Hydrostatic stiffness	Nm/rad	$3.42x10^9$
Total mass	kg	$11.8x10^6$
Rotor Diameter	m	126
Hub Height	m	90
Rotor Mass	kg	$110x10^3$
Nacelle Mass	kg	$240x10^3$
Cut-In, Rated, Cut-Out Wind Speed	m/s	3, 11.4, 25
Cut-In, Rated Rotor Speed	rpm	6.9, 12.1

Journal of Offshore Mechanics and Arctic Engineering. Received April 04, 2022;
Accepted manuscript posted September 01, 2022. doi:10.1115/1.4055552

Table 2: Natural frequencies and damping ratios of the two-rotor FOWT system computed through free-decay tests.

Degree of freedom	Natural frequency [Hz]	Damping ratio [%]
Surge	0.0075	8.73
Sway	0.0075	8.73
Heave	0.031	1.96
Roll	0.033	3.81
Pitch	0.033	3.81
Yaw	0.029	4.12

Journal of Offshore Mechanics and Arctic Engineering. Received April 04, 2022;
Accepted manuscript posted September 01, 2022. doi:10.1115/1.4055552

Table 3: Operational wind speeds associated with LQR controllers employed.

Control	U_{rel} $[m/s]$
LQR-A	3 - 10
LQR-B	11 - 12
LQR-C	13 - 25

Journal of Offshore Mechanics and Arctic Engineering. Received April 04, 2022;
Accepted manuscript posted September 01, 2022. doi:10.1115/1.4055552

Table 4: Steady-state operation points used for linearization.

		LQR-A	LQR-B	LQR-C
U_{rel}	m/s	9	11.3	13
β	rad	0.052	0.1	0.118

Journal of Offshore Mechanics and Arctic Engineering. Received April 04, 2022;
Accepted manuscript posted September 01, 2022. doi:10.1115/1.4055552

Table 5: LQR control weigths.

	$[Q]$	$[R]$
LQR-A	*diag(0, 0, 0, 0, 0, 0, 0, 0, 500, 1, 0, 0)*	*diag(100,100)*
LQR-B	*diag(0,0,0,0,500,500,0,0,2500,2500,0.01,0.01)*	*diag(200,200)*
LQR-C	*diag(0, 0, 0, 0, 5, 5, 0, 0, 5000, 5000, 1, 1)*	*diag(100,100)*

Journal of Offshore Mechanics and Arctic Engineering. Received April 04, 2022;
Accepted manuscript posted September 01, 2022. doi:10.1115/1.4055552

Table 6: LQR control gain scheduling.

	$[K]$
LQR-A	$\begin{bmatrix} 0,0,0,0,-0.0241,0.0241,0,0,1.2244,5.4343,0,0 \\ 0,0,0,0,0.0241,-0.0241,0,0,-1.2244,-5.4343,0,0 \end{bmatrix}$
LQR-B	$\begin{bmatrix} 0,0,0,0,-0.87,-0.38,0,0,1.929,6.52,0.0071,0 \\ 0,0,0,0,-0.38,-0.87,0,0,-1.929,-6.52,0,0.0071 \end{bmatrix}$
LQR-C	$\begin{bmatrix} 0,0,0,0,-1.617,1,0,0,5.04,-0.8838,0.1,0 \\ 0,0,0,0,1,-1.617,0,0,-5.04,0.8838,0,0.1 \end{bmatrix}$

Journal of Offshore Mechanics and Arctic Engineering. Received April 04, 2022;
Accepted manuscript posted September 01, 2022. doi:10.1115/1.4055552

Table 7: Major reference controller parameters.

		OC3 PI	PI-P
Proportional gain (yaw mitigation), K_{q_6}	-		1.5
Proportional gain at minimum blade-pitch setting, $K_P(0)$	s	0.00627	-
Integral gain at minimum blade-pitch setting, $K_I(0)$	-	0.00089	-
Maximum blade pitch rate	deg/s	8	-
Minimum blade pitch	deg	0	-
Maximum blade pitch	deg	90	-

Journal of Offshore Mechanics and Arctic Engineering. Received April 04, 2022;
Accepted manuscript posted September 01, 2022. doi:10.1115/1.4055552

Table 8: Environmental parameters.

U_{rel}	m/s	5-25
$Turb$		Kaimal
I		NTM B
$S(\omega)$		JONSWAP
H_s	m	6
T_p	s	10

Journal of Offshore Mechanics and Arctic Engineering. Received April 04, 2022;
Accepted manuscript posted September 01, 2022. doi:10.1115/1.4055552

List of Figures

Journal of Offshore Mechanics and Arctic Engineering. Received April 04, 2022;
Accepted manuscript posted September 01, 2022. doi:10.1115/1.4055552

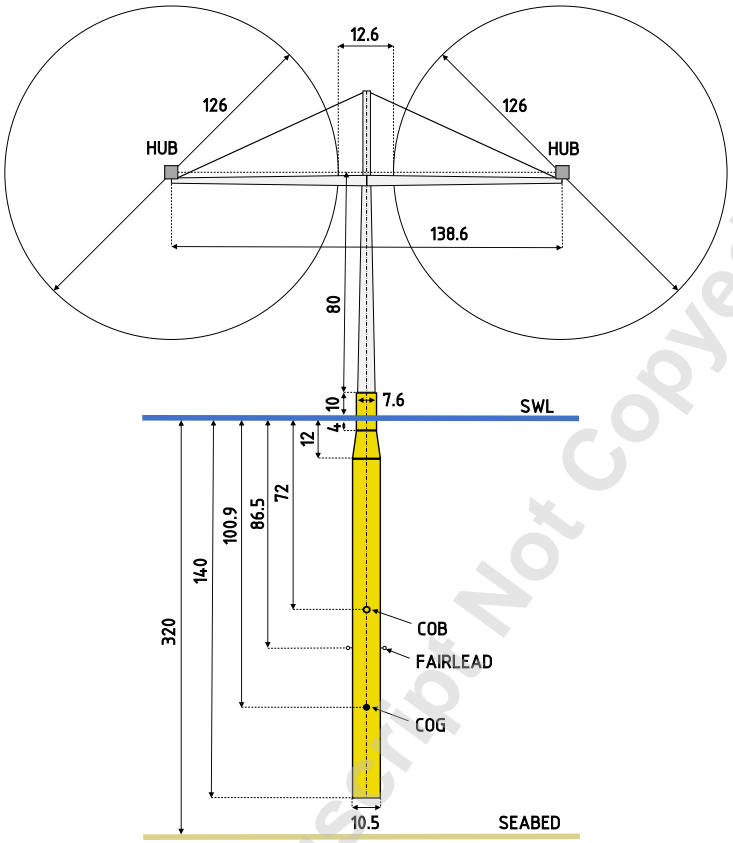

Figure 1: 2WT multi-rotor FOWT prototype presented in [11] and considered in this work (lengths in m).

Journal of Offshore Mechanics and Arctic Engineering. Received April 04, 2022;
Accepted manuscript posted September 01, 2022. doi:10.1115/1.4055552

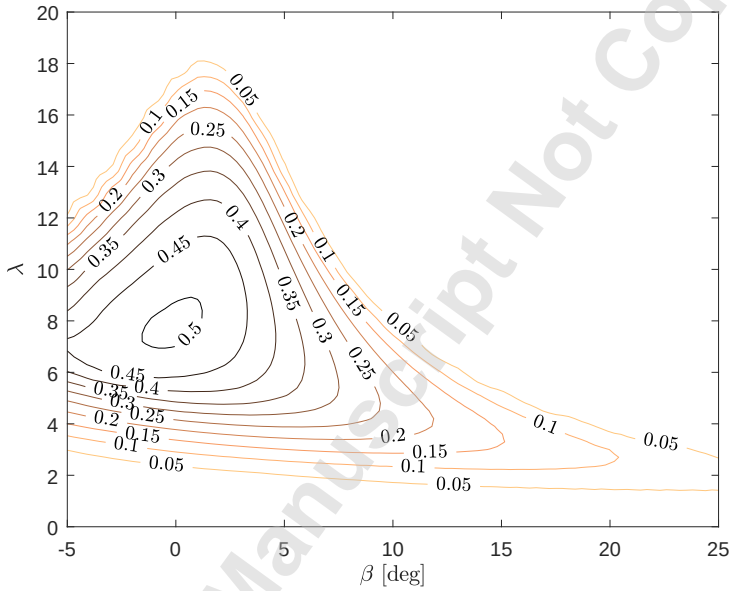

Figure 2: Power coefficient (C_P).

Journal of Offshore Mechanics and Arctic Engineering. Received April 04, 2022;
Accepted manuscript posted September 01, 2022. doi:10.1115/1.4055552

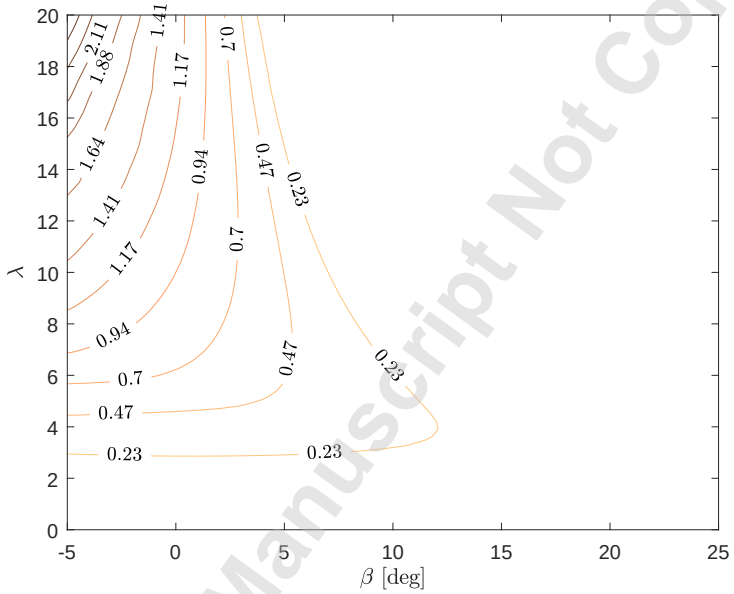

Figure 3: Thrust coefficient (C_T).

Journal of Offshore Mechanics and Arctic Engineering. Received April 04, 2022;
Accepted manuscript posted September 01, 2022. doi:10.1115/1.4055552

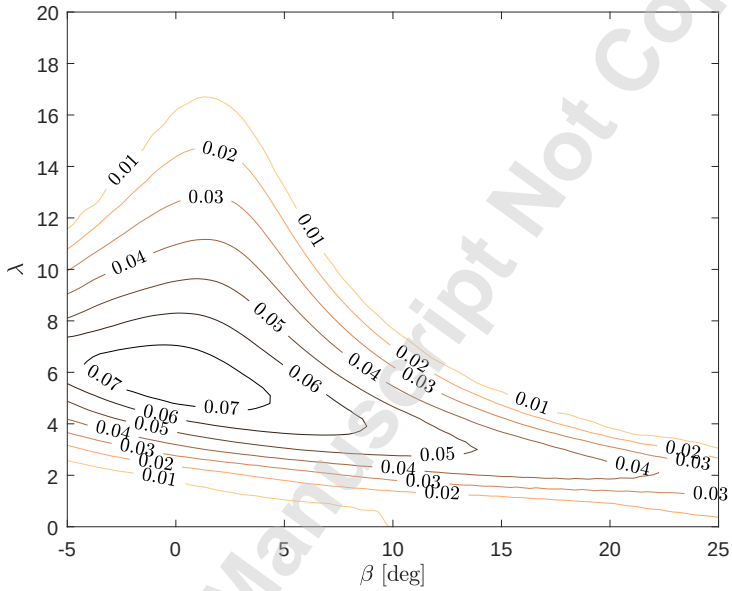

Figure 4: Torque coefficient (C_Q).

Journal of Offshore Mechanics and Arctic Engineering. Received April 04, 2022;
Accepted manuscript posted September 01, 2022. doi:10.1115/1.4055552

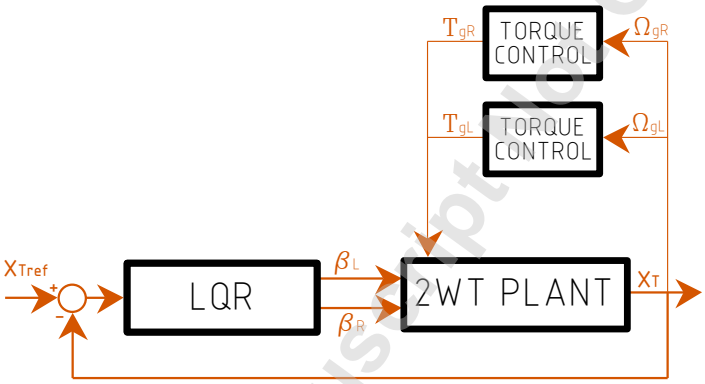

Figure 5: Control schematics.

Journal of Offshore Mechanics and Arctic Engineering. Received April 04, 2022;
Accepted manuscript posted September 01, 2022. doi:10.1115/1.4055552

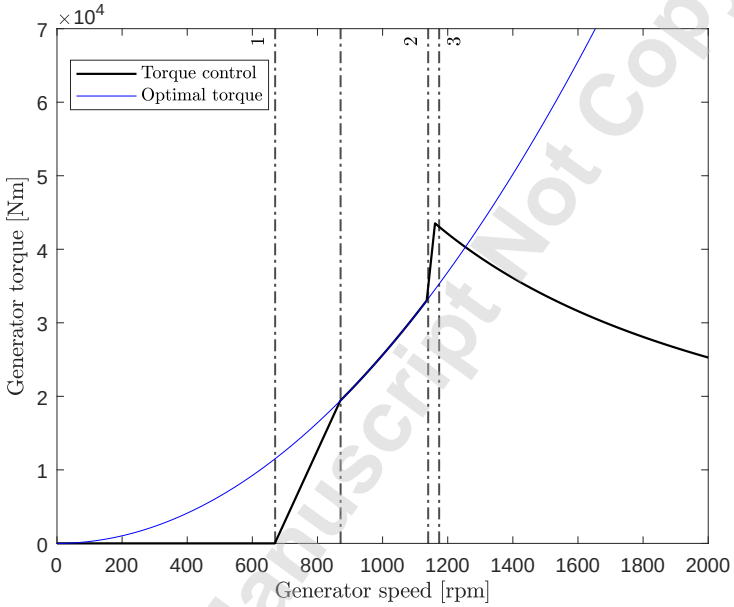

Figure 6: Generator torque control.

Journal of Offshore Mechanics and Arctic Engineering. Received April 04, 2022;
Accepted manuscript posted September 01, 2022. doi:10.1115/1.4055552

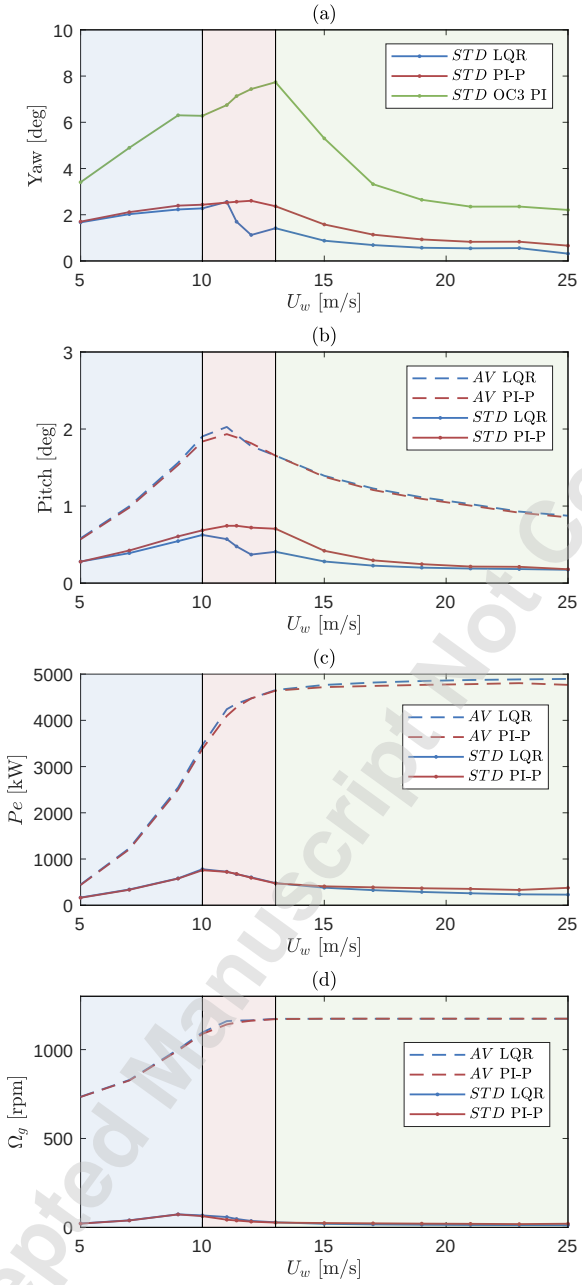

Figure 7: Performance of LQR and coupled PI-P controllers as a function of wind speed. Platform yaw response with OC3 PI controller is also included. Control regions associated with different LQR gain schedulings are highlighted with different box colors. Response given in terms of a) platform yaw STD, b) platform pitch motion, c) electric power, and d) generator speed. Only results relative to the left turbine are shown.

Journal of Offshore Mechanics and Arctic Engineering. Received April 04, 2022;
Accepted manuscript posted September 01, 2022. doi:10.1115/1.4055552

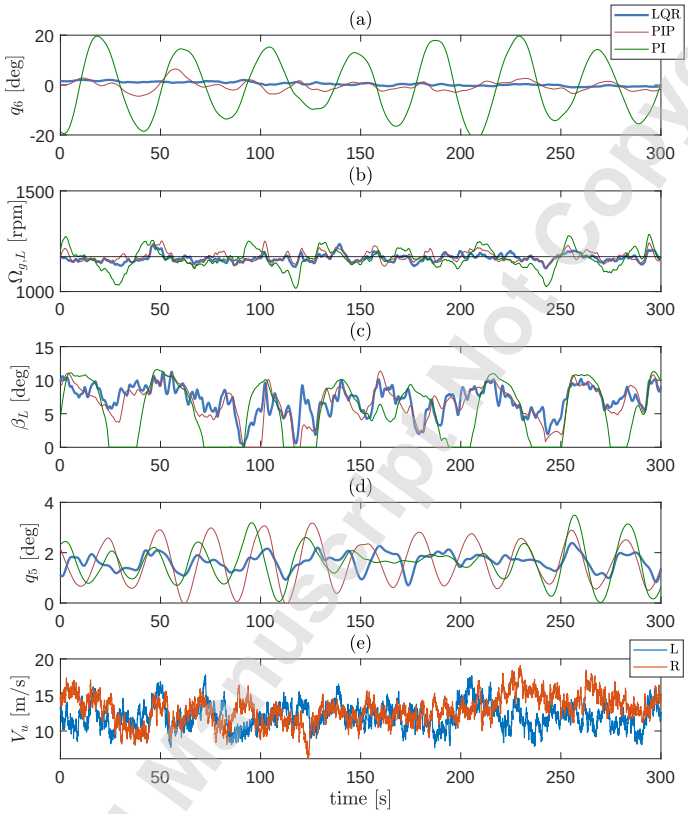

Figure 8: Above-rated 2WT response 300 s time series of a) platform yaw motion, b) generator speed, c) blade-pitch angle, and d) platform pitch motion for LQR (control LQR-C), baseline OC3 PI, and PI-P controllers. Mean wind speed 13 m/s. Only results relative to the left turbine are shown. Turbulent wind realizations at hubs are also depicted (e).

Journal of Offshore Mechanics and Arctic Engineering. Received April 04, 2022;
Accepted manuscript posted September 01, 2022. doi:10.1115/1.4055552

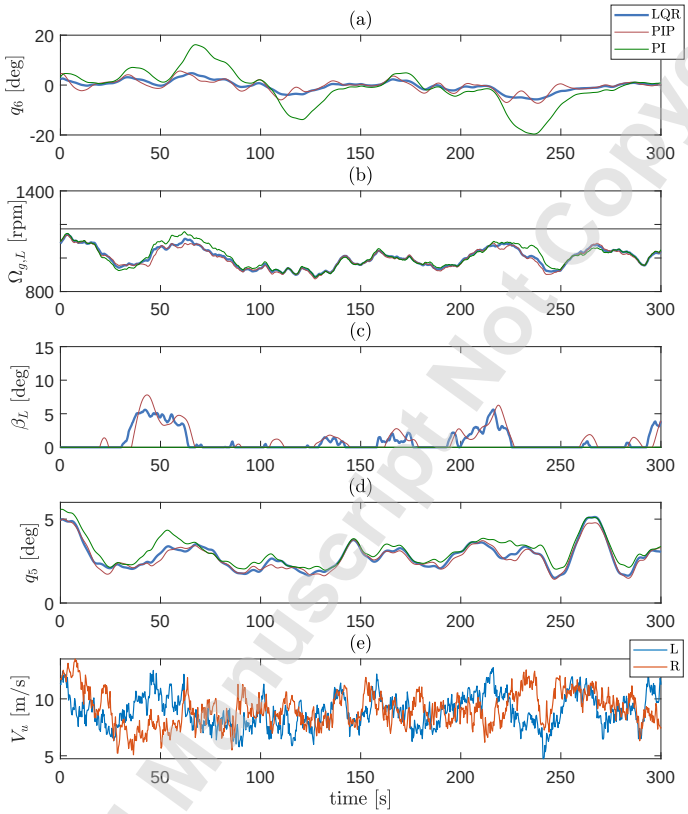

Figure 9: Below-rated 2WT response 300 s time series of a) platform yaw motion, b) generator speed, c) blade-pitch angle, and d) platform pitch motion for LQR (control LQR-A), baseline OC3 PI, and PI-P controllers. Mean wind speed 9 m/s. Only results relative to the left turbine are shown. Turbulent wind realizations at hubs are also depicted (e).

Journal of Offshore Mechanics and Arctic Engineering. Received April 04, 2022;
Accepted manuscript posted September 01, 2022. doi:10.1115/1.4055552

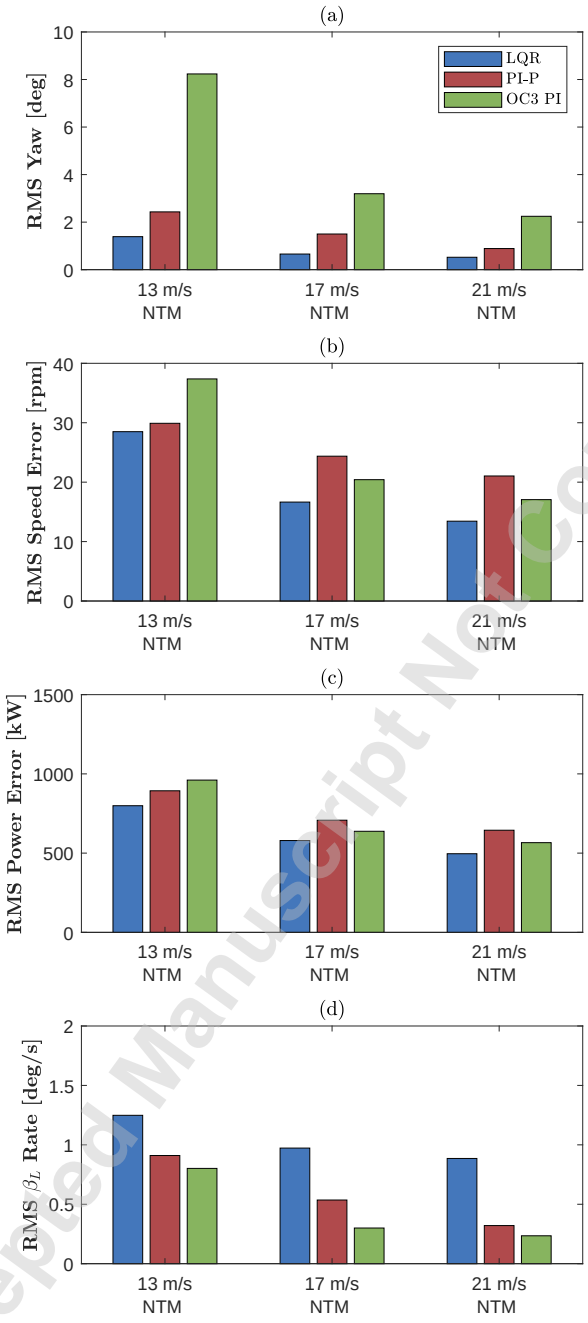

Figure 10: Performance comparison for LQR, baseline OC3 PI, and coupled PI-P controllers at above-rated wind speeds. RMS of a) platform yaw motion, b) generator speed error, c) electric power error, and d) blade-pitch rate. Only results relative to the left turbine are shown.

Journal of Offshore Mechanics and Arctic Engineering. Received April 04, 2022;
Accepted manuscript posted September 01, 2022. doi:10.1115/1.4055552

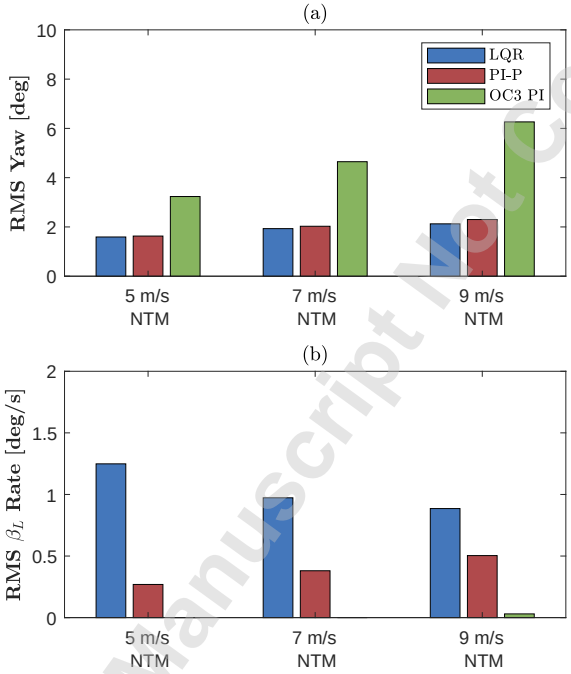

Figure 11: Performance comparison for LQR, baseline OC3 PI, and coupled PI-P controllers at below-rated wind speeds. RMS of a) platform yaw motion and b) blade-pitch rate. Only results relative to the left turbine are shown.